



STATISTICAL POWER-FLOW ANALYSIS OF AN IMPERFECT RIBBED CYLINDER

M. BLAKEMORE

Topexpress Ltd, 511 Coldhams Lane, Cherry Hinton, Cambridge CB1 3JS, England

J. WOODHOUSE

Cambridge University Engineering Department, Trumpington Street, Cambridge CB2 1PZ, England

AND

D. J. W. HARDIE

DERA Winfrith Technology Centre, Dorchester, Dorset DT2 8XJ, England

(Received 7 May 1998, and in final form 9 December 1998)

Prediction of the noise transmitted from machinery and flow sources on a submarine to the sonar arrays poses a complex problem. Vibrations in the pressure hull provide the main transmission mechanism. The pressure hull is characterised by a very large number of modes over the frequency range of interest (at least 100,000) and by high modal overlap, both of which place its analysis beyond the scope of finite element or boundary element methods. A method for calculating the transmission is presented, which is broadly based on Statistical Energy Analysis, but extended in two important ways: (1) a novel subsystem breakdown which exploits the particular geometry of a submarine pressure hull; (2) explicit modelling of energy density variation within a subsystem due to damping. The method takes account of fluid–structure interaction, the underlying pass/stop band characteristics resulting from the near-periodicity of the pressure hull construction, the effect of vibration isolators such as bulkheads, and the cumulative effect of irregularities (e.g., attachments and penetrations).

© 1999 Crown Copyright

1. INTRODUCTION

This paper is concerned with noise levels at sonar arrays which are positioned on the forward flanks and the bow of a submarine. Potentially significant noise sources can include the propulsor, other machinery internal to the submarine, and the external flow. The principal machinery sources are mostly sited well aft of the arrays. The estimation of the noise transmitted from these sources to the arrays, over a wide range of frequencies, poses a complex prediction problem. It is worth making three initial observations.

(1) For all these noise sources, the pressure hull itself provides the most important structural transmission path to the arrays, as opposed to any pathway through the internal structure such as decks. This is mainly due to the large impedance mismatch at all junctions with the pressure hull, combined with the

complex nature of these internal structures. (This internal “fuzzy structure” may, however, contribute to the effective structural damping of the pressure hull [1, 2]) On the pressure hull, both flexural-like waves and in-surface waves (compression and shear) provide potentially important transmission mechanisms.

(2) The pressure hull is made up of a cylindrical shell braced against external pressure by circumferential T-section frames. The frames are fairly regularly spaced axially, and they are substantial enough to present a significant impedance to the pressure hull. They produce a characteristic pass- and stop-band frequency variation of the structure-borne transmission [3, 4].

(3) The pressure hull is divided into a small number of separate sections by bulkheads, changes of diameter, or changes of frame spacing or geometry. These are all potentially significant reflectors of structure-borne energy incident in the pressure hull, and need to be taken into account in any predictive procedure.

In the discussion that follows, the combination of the pressure hull (including the frames) and reflectors such as bulkheads is considered, in the presence of an external fluid. The external fluid has three distinct effects [5]: mass loading of the structure; adding effective damping through radiation; and fluid short-circuiting of vibration attenuators, including the frames and bulkheads. The frequency range of interest may encompass the flat plate coincidence frequency, the frequency at which flexural wavelengths match acoustic wavelengths (see reference [5]). Radiation loss from flexural waves on the structure can occur below that frequency due to the effects of curvature and wave scattering by the frames. Indeed radiation damping tends to dominate intrinsic structural damping, producing loss factors typically in the region of 10^{-2} to 10^{-1} . Modal overlap is consequently high, and the global structure non-reverberant for flexural-like waves (though *local* build-up of reverberant energy remains a possibility).

The isolated reflectors mentioned in (3) above can be analysed by deterministic theory which assumes perfect cylindrical symmetry, and such analysis often suggests that it is possible to achieve very low transmission by suitable design. For example, it is possible to design different frame spacings for different sections of the submarine such that pass bands in one section coincide with stop bands in another. However, it is generally found in practice that the predicted low transmission is not attained. A mechanism for this will be suggested, whereby the reflector is “short-circuited” by the cumulative effect of small-scale irregularities in the structure, which produce a small but significant degree of coupling between different wavetypes. For long range transmission, it is essential to include such effects in the prediction methodology. In this paper a statistical approach to this problem is proposed, based on an analysis of power flow on a ribbed cylinder. One begins by reviewing the underlying dispersion characteristics of the corresponding perfectly regular structure.

2. DISPERSION CHARACTERISTICS OF A FLUID-LOADED RIBBED CYLINDER

The vibration transmission characteristics of an infinite regularly-framed rotationally-symmetric fluid-loaded thin cylindrical shell are considered. For

such a structure, it is possible to decompose the global problem into a set of independent one-dimensional problems, indexed by “angular order” $n = 0, 1, 2, \dots$. Each component of the solution then has circumferential behaviour like $\cos n\theta$ or $\sin n\theta$, where θ is the circumferential angle. The detailed theory was described and experimentally verified for the *in vacuo* case by Hodges *et al.* [3, 4].

Fluid loading is formally incorporated into the scheme by adding to the kinetic energy extra terms representing the response of the fluid to radial motion of the shell, as determined by the kinematic boundary condition. This incorporates both mass loading and radiation damping. The determination of the fluid-loaded transmission modes then involves the solution of a matrix eigenvalue problem. This cannot however be solved by standard matrix procedures due to the non-algebraic frequency dependency in the fluid-loading terms. Instead, a non-linear equation solver is adopted. For each transmission mode, several relevant quantities can be readily calculated from the eigensolution, including the frequency, group velocity, radiation loss factor, mode shape and admittance.

These propagation modes are indicated in Figure 1 on a frequency/angular order diagram. This figure is calculated using the geometric parameters of the model pressure hull which was studied by Hodges *et al.* [3, 4], now assumed to be immersed in water. Specifically, the figure shows the frequency/wavenumber spectrum for radial acceleration on an ideal fluid-loaded ribbed cylinder at a position six frame-bays remote from an assumed radial drive. To ensure that all flexural-like transmission modes contribute with similar levels, the drive is taken to be temporally white, and spatially white in the driven bay (i.e., “rain-on-the-roof” drive in one bay), and the response is calculated at a position within the frame bay which is not a simple fraction of the bay length (thus avoiding any obvious nodes). At each frequency and angular order in the diagram, a horizontal tick is plotted whose length is linearly related to the logarithm of the computed response, with a 40 dB dynamic range. Regions of heavy markings therefore identify the flexural-like pass bands of the structure.

The positions and widths of the pass and stop bands vary with angular order. This predicted pattern has been well validated by comparison with detailed model scale measurements [3, 4]. A full description of the pattern is beyond the scope of this paper, but note that sketches of mode shapes at a selection of points in the figure were shown in Figure 2 of reference [4] for the *in vacuo* case. The only aspect of the pattern which needs to be discussed here relates to the obvious qualitative difference between the left and right regions, separated in Figure 1 by the shaded region.

Consider first the problem of a single frame on an infinite cylinder. An incident propagating wave, of any type, will in general be partly reflected and partly transmitted by such a frame. A general theorem relating to vibration transmission and reflection by a symmetrical scatterer (like the frame) leads one to expect that, in the absence of damping, there will be certain frequencies at which perfect reflection occurs, and others at which perfect transmission occurs [6]. This is indeed found to be the case here, as is illustrated in Figure 2 which shows the transmission coefficient for flexural waves of angular order $n = 24$,

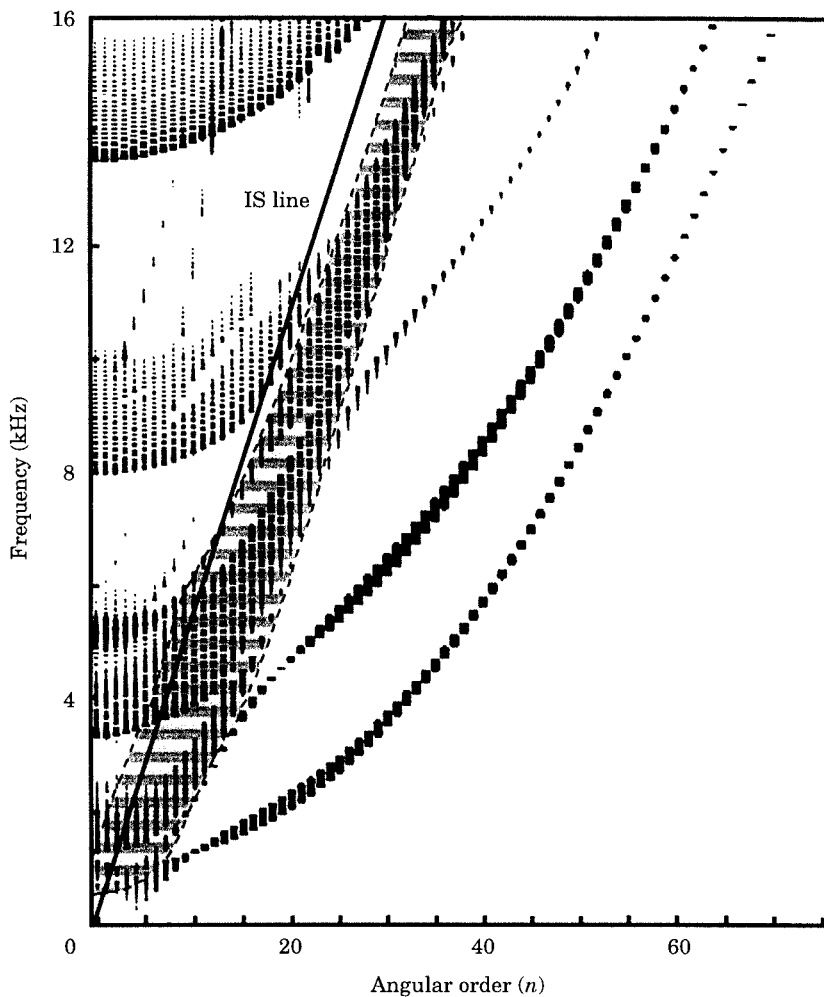


Figure 1. Pass- and stop-band structure for a typical ribbed cylinder geometry, which corresponds to the small-scale model studied by Hodges *et al.* [3, 4]. See text for detailed description.

plotted against frequency. At certain frequencies this falls to zero (perfect reflection), and at others it rises to unity (perfect transmission). These frequencies of perfect transmission are associated with “coincidence” between the trace wavenumber of predominantly-flexural waves in the shell and the wavenumber of flexural or torsional waves in the frame [7]. The frequencies of perfect transmission and perfect reflection vary in a systematic way with angular order. The shaded region of Figure 1 shows the trend. Specifically, the boundaries of the region follow the two frequencies of perfect reflection marked with arrows in Figure 2, and just inside the region are found two frequencies of perfect transmission. In terms of the behaviour of the periodically-ribbed cylinder, “perfect transmission” implies very strong coupling between adjacent bays so that the stop band width tends to be very small, while conversely

“perfect reflection” implies very weak coupling so that the pass-band width tends to be small.

One can now divide the propagation modes into four classes, which will form the basis of the later analysis. For wavenumber–frequency values to the left of the shaded region in Figure 1 the influence of the frames is inertia dominated. Here are found the “type L” flexural modes, which tend to have wide pass-bands and high axial group velocities (away from the edges of the pass bands), and usually also have high radiation damping. Conversely the “type R” modes to the right, where the influence of the frames is stiffness dominated, have narrow pass-bands. The frames are effective reflectors in this region so that the coupling between adjacent bays is weak. These modes typically have group velocity vectors which are predominantly circumferential, so that the axial component is small. They also have low radiation damping. Type L and type R modes, despite their differences, turn out to have spatial attenuation rates which are generally comparable, and rather high, as will be shown later. The transition region between the two is associated with “type C” modes (the shaded region on Figure 1), and these are significantly different in their behaviour. They have the broadest pass bands of all flexural modes, and they also have rather low radiation damping, so that they tend to have relatively low spatial attenuation rates. Finally it is useful to group all in-surface modes, including compression and shear types, into a single class, designated “IS”. These are confined to the region to the left of the relevant line on Figure 1. Formally, they are defined as those propagation modes in which more than half the strain energy is associated with in-surface motion rather than bending. They have the highest group velocities of all, and very low spatial attenuation rates. Any mode having more than half its strain energy associated with bending deformation is

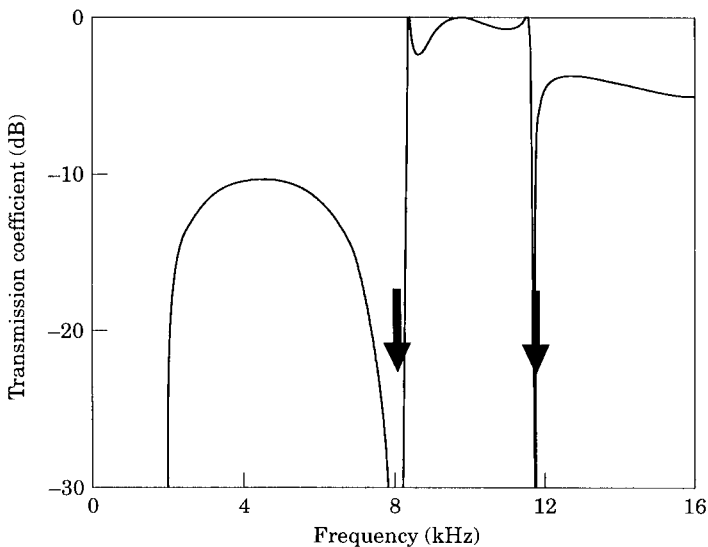


Figure 2. Transmission coefficient across a single frame on an infinite unribbed cylinder, for $n = 24$. Notice that perfect transmission occurs at certain frequencies, and perfect reflection at others. The frequencies marked with arrows form the boundaries of the “Type C” modes for this value of n .

TABLE 1
Qualitative characteristics of the four groups of waves on a ribbed cylinder

Type	L	C	R	IS
Pass band width	wide	wide	narrow	very wide
Axial group velocity	fast	fast	slow	very fast
Radiation damping	high	fairly low	low	moderate
Spatial decay	fast	fairly slow	fast	very slow

classified as type L, type C or type R depending on where it falls in Figure 1. The key properties of the four mode types are summarised in qualitative form in Table 1.

3. STATISTICAL MODELLING

3.1. REALISTIC STRUCTURES

This deterministic model of a perfectly regular structure is adequate to represent the characteristics of transmission over a few frame bays. However for long-range transmission on a realistic structure, a number of complicating factors need to be taken into account: (1) the finite length of the structure; (2) the effect of isolated reflectors (e.g., bulkheads); (3) the effect of irregularities (e.g., attachments, pressure hull penetrations, and random constructional imperfections).

As discussed earlier, the transmission of flexural waves past the isolated reflectors may be predicted to be quite small on the basis of idealised modelling which assumes the cylinder is perfect. In this case, (3) above becomes crucially important—although the scattering from an individual irregularity is typically small, the cumulative effect is significant, producing a weak “diffusive” scatter between angular orders which can short circuit the theoretical low transmission. Of course all the above effects can in principle be modelled deterministically, by augmenting the idealised theory. However this deterministic approach either loses accuracy (because the assumptions made in order to make the problem tractable become invalid) or the degree of complexity in the problem becomes unmanageable. It is inevitable then that one considers methodologies where the irregularities and their effects are represented statistically in some way.

3.2. SUBSYSTEM BREAKDOWN

One starts by considering the standard statistical approach for structural vibration problems—Statistical Energy Analysis or SEA (see references [8, 9]). Within SEA, a structure is first divided into discrete subsystems within which response levels are assumed to be homogeneous. Linear equations are then set up to represent energy exchange and balance between these subsystems. By solving these, it is possible to deduce the response level within each subsystem in terms of the energy input from excitation sources.

Perhaps the most obvious subsystem breakdown of the pressure hull would be into individual frame bays, frames etc. However it is well known that a

breakdown of a periodic or near-periodic structure into periodic elements in this way produces an SEA model with qualitatively the wrong behaviour (see references [8, 9]), essentially because SEA neglects coherence effects which are crucial in determining the transmission characteristics of the periodic structure.

The present approach is to take a macro-scale view of the pressure hull structure, regarding the ribbed cylinder as a kind of composite material with rather complicated dispersion characteristics for vibration transmission. One can then choose physical subsystems which are many frame bays in length. There are now the usual conflicting considerations with regard to SEA—breakdown into small subsystems produces high resolution, but larger subsystems may be necessary in order to satisfy the SEA requirement for high modal density and overlap per subsystem. Here a derivative of SEA will be discussed—the statistical power-flow method—which attempts to satisfy both objectives, using physical subsystems which are as large as is sensible, but allowing for variation of levels within each subsystem consistent with the known transmission and radiation characteristics of the various wavefields.

The first breakdown is into physical sections or “chunks”. There may be half a dozen or so chunks to a submarine, and they are what might most easily be inferred from a drawing, without any reference to vibration—the Main Machinery Compartment or Reactor Compartment, for example. They relate to sections of pressure hull in which one would expect no sudden changes in vibration levels or transmission characteristics. A chunk boundary would be placed at a significant reflector (e.g., a bulkhead) or a change in transmission characteristics (due to a change in mean frame spacing or shell thickness, say). Ideally a chunk should be many bays long, so that the infinite-cylinder dispersion characteristics can become established within a chunk. Such evidence as is available suggests that “many bays long” in this context means “at least three bays long”. This estimate is based on simulation experiments to establish the minimum number of periodically placed ribs on an otherwise unribbed cylinder required in order to see evidence of the stop/pass band structure. A further breakdown into different wave types is now necessary, to represent in some way the wide range of transmission characteristics. Again, an extremely fine subdivision into individual propagation modes and individual angular orders is entirely feasible. However a coarser breakdown into four wavetypes has been chosen. These are the in-surface (IS) modes and the flexural L-, C- and R-modes discussed earlier.

The statistical model predicts expected response levels based on averaged quantities relating to the dynamical properties of the structure and fluid. These average quantities are easily calculated from the characteristics of the transmission modes of the ideal fluid-loaded structure. The ribbed-cylinder model allows these modes to be calculated over a discrete array of values for n and Bloch wavenumber q (see Hodges *et al.* [3]). The definition of the Bloch (or Floquet) wavenumber is that the bay-to-bay phase change in a travelling wave is $\exp[iqd]$ where d is the frame spacing. In a structure N_q bays in length, the number of normal modes within each pass band will be N_q . To calculate an approximation to these modes, the Bloch wavenumber is allowed to take N_q

discrete values equally spaced between zero and the Nyquist wavenumber π/d . The characteristics of each transmission mode are calculated, including the frequency, group velocity, radiation loss factor, and mode shape information (within a bay).

To perform the averaging, frequency bins are first selected: in the case to be presented here these are bands of constant 500 Hz bandwidth. Average quantities are accumulated in these bins for each wavetype (L, C, R and IS) by looping over all the transmission modes. For each mode, the corresponding type is established, as discussed above, by reference to its strain energy distribution, its frequency, and its angular order. The average modal density per frame bay $\hat{N}(f)$ (f being frequency in Hz) is obtained simply by counting the modes in each bin and dividing by the bin width and by N_q . (It is convenient to work in terms of an axial distance \hat{x} which is non-dimensionalised on the bay spacing d . All quantities based on this non-dimensional distance will be denoted by a circumflex.) The results become independent of N_q provided it is sufficiently large. For computational purposes a value $N_q = 48$ was used, large enough to sample the dispersion characteristics adequately.

Next, the power input must be calculated. There is a standard result for the average power input into a spatially homogeneous system without fluid loading (see for example Lyon and De Jong [9], equation (2.2.22)): the input conductance G is given by

$$G(f) = N(f)/4M, \quad (1)$$

where $N(f)$ is modal density (in modes/Hz) and M is the mass of the structure. This result must be modified for the present problem, in two respects. In the presence of significant fluid loading the effective mass will vary from mode to mode because of local fluid motion, and this must be taken into account. Also, the ribbed cylinder is not homogeneous, and one wishes to allow the possibility of, for example, forcing on the frames.

An input conductance for any particular transmission mode of the structure can be defined as the power input per bay resulting from driving the structure with the corresponding generalised force applied randomly in time. The average input conductance of each particular mode ‘‘type’’, denoted by G_L , G_C , G_R and G_{IS} , is then the average of this quantity over all modes of the appropriate type within the band. Equation (1) applies to G_α in place of G , provided $N(f)/M$ is interpreted to mean the mode-by-mode aggregate over type- α modes, allowing for the varying effective modal mass, where the subscript α denotes any of the mode types L, C, R or IS.

To allow for a particular pattern of forcing, this formula can be modified by including a dimensionless mode-shape factor. For example, for point forcing with mean squared amplitude $|F|^2$ at position \mathbf{x} within the frame bay and in direction \mathbf{e} , the power input to mode type α is given approximately by

$$\Pi_m = |F|^2 G_\alpha \zeta(\mathbf{x}, \mathbf{e}), \quad (2)$$

where the factor $\zeta(\mathbf{x}, \mathbf{e})$ is computed as the mean square over the modes in the

band of the mode shape at position \mathbf{x} and in direction \mathbf{e} (where mode shapes are assumed to be normalised to have a spatial mean-square of unity). The quantity $\xi(\mathbf{x}, \mathbf{e})$ can be used in a reciprocal manner to obtain responses at a specific site within a frame bay from the SEA energy. Thus the mean square velocity response at position \mathbf{x} and in direction \mathbf{e} is given by

$$[\text{Energy per bay}/\text{Effective mass per bay}]\xi(\mathbf{x}, \mathbf{e}). \quad (3)$$

Other quantities required by the statistical models, such as group velocity \hat{c}_α and radiation loss factor $\eta_\alpha^{(rad)}$, are calculated as simple averages of the individual modal quantities. The contribution to damping from structural effects is assumed to be constant, a loss factor $\eta_{struct} = 0.005$ being used for all wavetypes, so that the total loss factor for modes of type α is

$$\eta_\alpha = \eta_{struct} + \eta_\alpha^{(rad)}. \quad (4)$$

A particularly significant quantity derived in this way is the average spatial attenuation rate associated with modes of type α :

$$\hat{\lambda}_\alpha = \eta_\alpha \omega / \hat{c}_\alpha. \quad (5)$$

This quantity is plotted against frequency in Figure 3. The values cover a very wide range, so to give a clear view the vertical scale is doubly logarithmic: it shows attenuation in (decibels per frame bay) on a logarithmic scale. In broad terms, this confirms the qualitative account given in Table 1. The type L and type R modes tend to have the fastest attenuation rates, sometimes remarkably fast. The type C modes are, on the whole, more slowly attenuated, and the type IS modes only attenuate very slowly indeed.

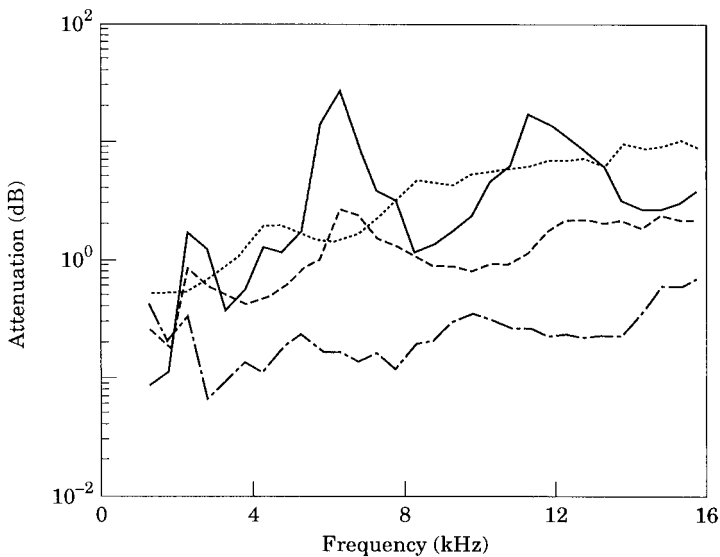


Figure 3. Spatial attenuation rate along the fluid-loaded ribbed cylinder, in dB per frame bay: —, type L; ----, type C; ····, type R; -·-·-, type IS.

3.3. POWER-FLOW ANALYSIS WITHOUT COUPLING

The slightly unusual subsystem breakdown defined above could, of course, be used with standard SEA. SEA parameters like modal densities and coupling loss factors are easily computed from the deterministic model discussed above. The SEA equations are stated at the end of this subsection. The difficulty for SEA is that many of the flexural subsystems are non-reverberant, largely due to the high rates of radiation damping provided by the external fluid. Thus the assumption of homogeneous response within a subsystem—intrinsic to SEA—is invalid in principle (although the extent of error thus incurred is not obvious without calculation).

Instead, for these quasi-one-dimensional subsystems, it turns out to be quite easy to implement an analysis of power flow which ignores phase information but is otherwise in a certain sense “exact”. This theory corresponds to the infinite limiting case of the “ASEA” sequence of approximations defined by Heron [10]. Consider two “chunks” of the pressure hull, coupled end-to-end through a bulkhead, each chunk carrying four subsystems. Since each chunk is a spatially uniform section of ribbed cylinder, then a theory which ignores phase only requires two parameters to specify the complete energy field in any one subsystem: the power flows in left-travelling and right-travelling “energy waves”. For definiteness, define the vectors \mathbf{L}_j and \mathbf{R}_j such that the left-travelling power flows in the j th chunk associated with the various internal subsystems are given at the right end by \mathbf{L}_j , and the corresponding right-travelling power flows at the left end by \mathbf{R}_j . Each of these “energy waves” will decay exponentially as it travels, at the spatial rate $\hat{\lambda}_x$ defined in equation (5). Apart from “near fields” around any localised energy source, the energy field in a given subsystem can be described exactly (within the context of a theory ignoring phase) as a linear combination of these two exponential basis functions.

It is now straightforward to obtain a closed set of equations for these power flows, by considering the reflection and transmission behaviour at the junction, together with perfectly reflecting boundaries at the ends of the system. Some energy input is needed, of course. The simplest way to include this for a first examination of the results of this theory is to inject power at one end of the system at a known rate, and solve for the resulting distribution of energy density over the whole system. The system is illustrated schematically in Figure 4.

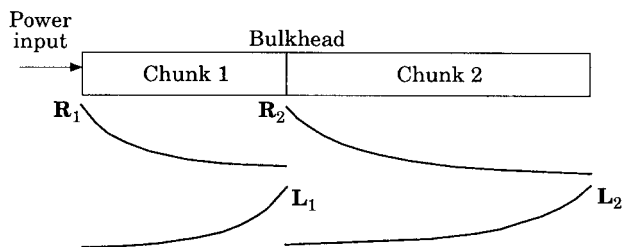


Figure 4. Schematic diagram of two-chunk system, and basis functions for “energy waves”.

Power flow associated with the different subsystems has different rates of exponential decay with distance. The amplitudes of the power flows by the time they reach the far end of the chunks can thus be represented by two diagonal matrices $\mathbf{\Lambda}_1, \mathbf{\Lambda}_2$ such that, for example, the right-travelling energy in chunk 1 has a vector of power flows at the right end (i.e., the bulkhead) of $\mathbf{\Lambda}_1 \mathbf{R}_1$. The elements of these matrices are simply given in terms of the exponential rates $\hat{\lambda}_\alpha$ and the lengths of the chunks \hat{D}_j .

Define the power input to be a vector \mathbf{P} —for definiteness, assume that the power input is broadband, uniformly distributed in frequency over a band centred at f Hz and of bandwidth B Hz. For simplicity of presentation, assume that the infinite system characteristics of chunk 2 are the same as those of chunk 1, so that, for example, the values of \hat{N}_α and \hat{c}_α are the same. Reflection and transmission at the bulkhead can then be characterised by just two matrices, $\boldsymbol{\rho}, \boldsymbol{\tau}$ respectively. (Extending the theory to the more general case is straightforward, but requires distinct reflection and transmission matrices for waves incident from the two directions.) Note that the matrix $\boldsymbol{\rho}$ is symmetric, while the matrix $\boldsymbol{\tau}$ satisfies

$$\hat{N}_\alpha \hat{c}_\alpha \boldsymbol{\tau}_{\alpha\alpha'} = \hat{N}_{\alpha'} \hat{c}_{\alpha'} \boldsymbol{\tau}_{\alpha'\alpha}. \quad (6)$$

The equations of energy flux balance are then as follows:

$$\begin{aligned} \mathbf{R}_1 &= \mathbf{\Lambda}_1 \mathbf{L}_1 + \mathbf{P}, \\ \mathbf{L}_1 &= \boldsymbol{\rho} \mathbf{\Lambda}_1 \mathbf{R}_1 + \boldsymbol{\tau} \mathbf{\Lambda}_2 \mathbf{L}_2, \\ \mathbf{R}_2 &= \boldsymbol{\tau} \mathbf{\Lambda}_1 \mathbf{R}_1 + \boldsymbol{\rho} \mathbf{\Lambda}_2 \mathbf{L}_2, \\ \mathbf{L}_2 &= \mathbf{\Lambda}_2 \mathbf{R}_2. \end{aligned} \quad (7)$$

It is straightforward to solve this set of linear equations, and hence find the energy distribution across the whole system. Examples will be shown shortly.

To relate these power flows to the subsystem energies of an SEA model, first define a quantity $T_\alpha(\hat{x})$ for each subsystem α at axial position \hat{x} , derived from the sum of the local power flows in the two directions:

$$T_\alpha(\hat{x}) = [R_\alpha e^{-\hat{\lambda}_\alpha \hat{x}} + L_\alpha e^{-\hat{\lambda}_\alpha (\hat{D}_j - \hat{x})}] / \hat{c}_\alpha \hat{N}_\alpha B. \quad (8)$$

This quantity will be referred to as the “temperature” of the subsystem at position \hat{x} since its spatial average

$$\bar{T}_\alpha = \frac{1}{\hat{D}_j} \int_0^{\hat{D}_j} T_\alpha(\hat{x}) \, d\hat{x} \quad (9)$$

is the usual SEA “temperature”, or mean energy per mode of the subsystem in chunk j . The total subsystem energy is then

$$E_\alpha = \bar{T}_\alpha \hat{D}_j \hat{N}_\alpha B. \quad (10)$$

For reference, the standard SEA equations are

$$\Pi_\alpha = \eta_\alpha \omega E_\alpha + \sum_{\alpha' \neq \alpha} \omega (\eta_{\alpha\alpha'} E_\alpha - \eta_{\alpha'\alpha} E_{\alpha'}), \quad (11)$$

where Π_α is the power input to subsystem α and $\{\eta_{\alpha\alpha'}\}$ are the coupling loss factors, and where the subscripts α, α' are now to be understood to range over each subsystem within each chunk of the whole system. The coupling loss factors can be derived in the usual way from the reflection and transmission coefficients at the bulkhead: for two subsystems in the same chunk j

$$\eta_{\alpha\alpha'} = \rho_{\alpha\alpha'} \hat{c}_\alpha / 2\omega \hat{D}_j \quad (\alpha \neq \alpha'), \quad (12)$$

while for subsystems α in chunk j and α' in an adjacent chunk k separated by the bulkhead,

$$\eta_{\alpha\alpha'} = \tau_{\alpha\alpha'} \hat{c}_\alpha / 2\omega \hat{D}_j. \quad (13)$$

3.4. POWER-FLOW ANALYSIS WITH COUPLING

Before showing any example calculations, a development of the theory to allow for the scattering effects of irregularities is discussed. Motivated by SEA, the proposed approach uses a heat-diffusion analogy between the parallel energy paths within each chunk. Some “leakage” between the paths at a rate proportional to the local difference of “temperatures” is allowed. For clarity of exposition, consider just two such coupled paths. Recall that the right sides of the corresponding SEA equations take the form

$$\eta_1 \omega E_1 + \omega (\eta_{12} E_1 - \eta_{21} E_2) \quad (14)$$

and

$$\eta_2 \omega E_2 + \omega (\eta_{21} E_2 - \eta_{12} E_1), \quad (15)$$

where SEA reciprocity requires that

$$\omega \hat{N}_1 \eta_{12} = \omega \hat{N}_2 \eta_{21} = \beta_{12} \quad (\text{say}). \quad (16)$$

One wishes to replace these with equations representing distributed coupling along the length of the chunk. The first stage is to write them in terms of the average “temperatures” \bar{T}_1 and \bar{T}_2 :

$$\eta_1 \omega \hat{N}_1 \bar{T}_1 + \beta_{12} (\bar{T}_1 - \bar{T}_2) \quad (17)$$

and

$$\eta_2 \omega \hat{N}_2 \bar{T}_2 + \beta_{12} (\bar{T}_2 - \bar{T}_1), \quad (18)$$

(where a common factor of the length of the chunk has been removed). Now replace the average temperatures with the spatially-varying temperatures, and, by

analogy with heat diffusion, write

$$\begin{aligned}
 C_1 \partial^2 T_1 / \partial \hat{x}^2 &= \Delta_1 T_1 + \beta_{12} (T_1 - T_2) \\
 C_2 \partial^2 T_2 / \partial \hat{x}^2 &= \Delta_2 T_2 + \beta_{12} (T_2 - T_1),
 \end{aligned}
 \tag{19}$$

where

$$\Delta_1 = \omega \eta_1 \hat{N}_1, \quad \Delta_2 = \omega \eta_2 \hat{N}_2
 \tag{20}$$

and C_1, C_2 are effective diffusivities. These diffusivities are determined by the requirement that, in the absence of the coupling term, each path should have the correct rate of spatial decay, as provided by the deterministic model. This requires

$$C_1 = \hat{c}_1^2 \hat{N}_1^2 / \Delta_1, \quad C_2 = \hat{c}_2^2 \hat{N}_2^2 / \Delta_2
 \tag{21}$$

in terms of the averaged group velocities \hat{c}_1, \hat{c}_2 .

The coupling term involves the constant β_{12} whose value, in practice, would probably be determined empirically by matching the length-scales of breakthrough energy transport to those found from measurements. An experimental methodology for such measurements would follow the work described by Hodges *et al.* [4]—the vibration field at different axial distances from a localised excitation could be decomposed into separate angular orders, and a picture built up experimentally which would correspond to, for example, Figure 7 below.

Generalised in the obvious way to allow for the four paths (or subsystems) per chunk, these equations can be written

$$\begin{aligned}
 &\begin{bmatrix} C_1 & 0 & 0 & 0 \\ 0 & C_2 & 0 & 0 \\ 0 & 0 & C_3 & 0 \\ 0 & 0 & 0 & C_4 \end{bmatrix} \begin{bmatrix} T_1'' \\ T_2'' \\ T_3'' \\ T_4'' \end{bmatrix} \\
 &= \begin{bmatrix} \Delta_1 + \beta_{12} + \beta_{13} + \beta_{14} & -\beta_{12} & -\beta_{13} & -\beta_{14} \\ & -\beta_{12} & \ddots & \dots \\ & -\beta_{13} & \vdots & \ddots \\ & -\beta_{14} & \vdots & \vdots \end{bmatrix} \begin{bmatrix} T_1 \\ T_2 \\ T_3 \\ T_4 \end{bmatrix}.
 \end{aligned}
 \tag{22}$$

But these are just the familiar equations for a four-degree-of-freedom vibrating system, with spatial derivatives in place of time derivatives, and with the two matrices on the left- and right sides playing the roles of “mass” and “stiffness” matrices. One can solve them by a “modal” transformation. The (generalised) eigenvalues of this pair of real, symmetric matrices give the spatial decay rates (squared) of the eigenvector combinations of energy levels in the various subsystems. If one constructs the matrix \mathbf{Q} whose columns are the eigenvectors

(normalised with the “mass matrix”, i.e., the diagonal matrix of diffusivities), then it can be used to map energy vectors into and out of these eigenvector combinations.

The result is that the analysis of the previous subsection carries over directly to this new case, provided only that one replaces the matrices $\mathbf{\Lambda}_1, \mathbf{\Lambda}_2$ by the combinations $\mathbf{Q}\mathbf{\Lambda}_1\mathbf{Q}^{-1}, \mathbf{Q}\mathbf{\Lambda}_2\mathbf{Q}^{-1}$, where the diagonal matrices $\mathbf{\Lambda}_1, \mathbf{\Lambda}_2$ here are calculated like the earlier ones, but using the eigenvalues for the decay rates. This formalises the translation into and out of modal co-ordinates in order to calculate the energy decay factors from end to end of the chunks.

4. EXAMPLE CALCULATIONS

For the purposes of illustration, a submarine structure consisting of two “chunks” of pressure hull separated by a bulkhead (modelled as a thin flat plate) will be considered. The length of chunk A will be $\hat{D}_A = 10$ frame bays, and that of B will be $\hat{D}_B = 15$ bays. A normalised input of 1 W/Hz will be assumed into each of the four subsystems of chunk A at the end remote from the bulkhead. The ribbed cylinder geometry corresponds to the small-scale model studied by Hodges *et al.* [3, 4].

The spatial average of the SEA temperature (energy per mode \bar{T}_j) within each of the four subsystems of chunks A and B is plotted in Figures 5(a–d), for the different subsystem types. Each graph displays results calculated using both “standard” SEA and the statistical power flow method without “leakage” coupling. On each graph the two predictions for chunk A (the driven section) are virtually indistinguishable. However within chunk B very large differences are observed, particularly for types R and C, corresponding to transmission modes having the most rapid spatial decay. In effect standard SEA is assuming that the energy incident on the chunk boundary is the same as the spatially averaged result. This is much greater than is actually the case (because of the rapid rate of spatial decay in some subsystems). Therefore a greater transfer of energy into chunk B is predicted, with consequently higher estimated levels.

These results may be compared directly with those in Figures 6(a–d), which show the same comparison calculated with non-zero values for the coupling parameters β_{jk} . Purely for illustrative purposes these coupling terms are given values which are a constant multiple of $(\hat{N}_j + \hat{N}_k)\omega\eta_{struct}$, in terms of the damping rate η_{struct} due to structural damping alone, which is set at a constant value 0.005 for all subsystems. This models “a little coupling of everything to everything”. The diagonal terms of the matrix appearing on the right side of equation (22) also contains the contribution from radiation damping, which varies with mode type and with frequency, and is in general much bigger than the structural contribution.

The coupling value used to compute Figure 6 is only $\beta_{jk} = (\hat{N}_j + \hat{N}_k)\omega\eta_{struct}/1000$. Even with this tiny amount of coupling, the very low levels predicted in chunk B for types R and C are substantially increased. The main mechanism for this is that the bulkhead forms only a very weak reflector for IS waves, and to a lesser extent for type L waves. Energy transmits into

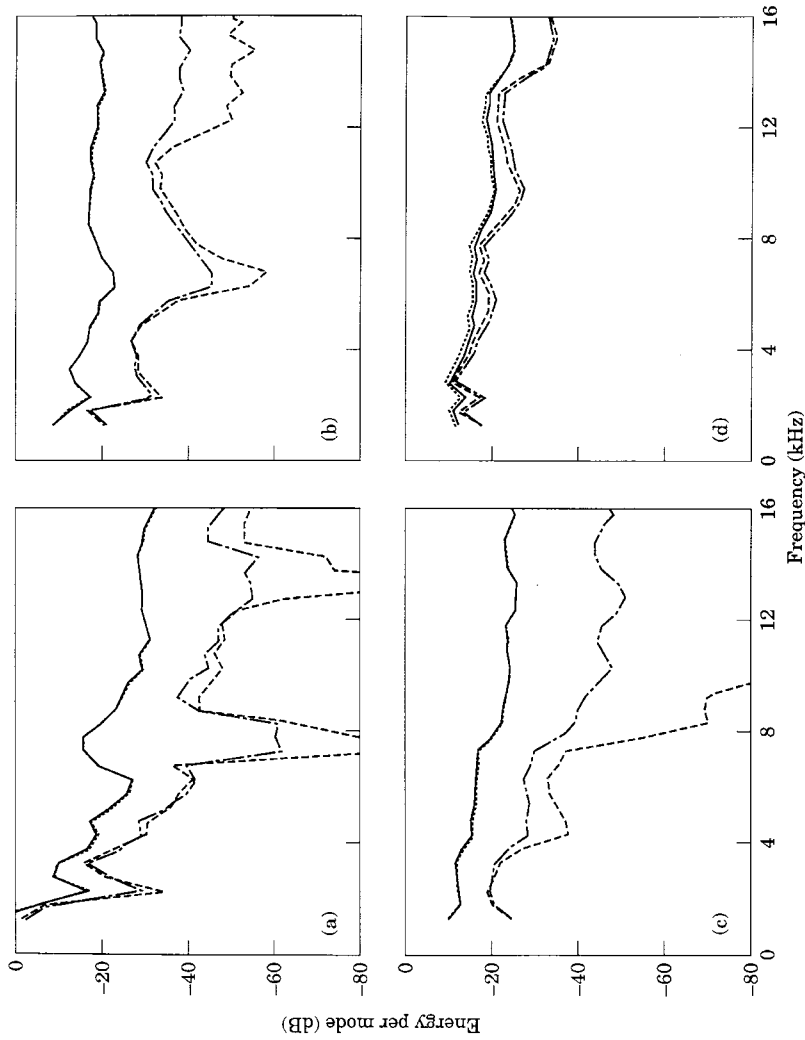


Figure 5. Comparison of power-flow modelling with SEA, in the absence of leakage coupling for (a) type L modes; (b) type C modes; (c) type R modes; (d) type IS modes. \cdots , chunk A, SEA; $-\cdot-\cdot-$, chunk B, SEA; $---$, chunk A, power flow; $----$, chunk B, power flow.

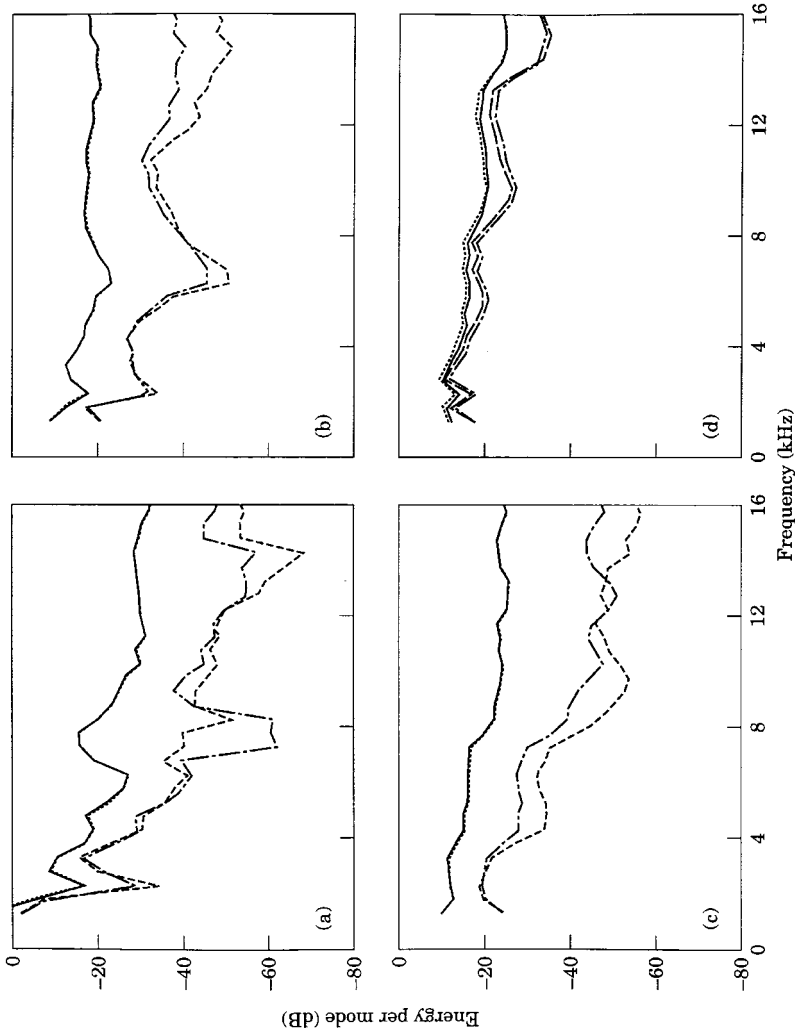


Figure 6. Comparison of SEA with power-flow modelling including constant leakage coupling $\beta_{jk} = (\hat{N}_j + \hat{N}_k)\omega\eta_{struct}/1000$, for (a) type L modes; (b) type C modes; (c) type R modes; (d) type IS modes. \cdots , chunk A, SEA; $-\cdot-\cdot-$, chunk B, SEA; $-----$, chunk A, power flow; $-----$, chunk B, power flow.

chunk B by these mechanisms, then can scatter back into types R and C. By the far end of chunk B, the SEA temperatures of types R and C had been raised, due to the coupling, to the extent where they were comparable with that of type L. Comparison of Figures 5 and 6 might suggest that the presence of irregularity brings the behaviour more in line with the predictions of “traditional” SEA. This is a misleading interpretation. SEA overpredicts the response in chunk B when the fields are non-reverberant, a conclusion not altered by irregularity. The effect of leakage coupling is to raise the levels in chunk B by an entirely different mechanism, not included in the SEA model. If it were to be included (in some average sense), the SEA predictions would diverge further from the power-flow predictions.

To gain some physical insight into the effect of coupling, some plots of spatial distribution of temperature $T_j(x)$ are presented. The temperature is plotted at each bay of the structure. The bulkhead is at the end of bay 10, and an obvious drop of levels occurs there. Figure 7(a) and (b) show two representative results without coupling, for two different frequency bands. Figures 7(c) and (d) show the results for the same frequency band as Figure 7(b), with coupling $\beta_{jk} = (\hat{N}_j + \hat{N}_k)\omega\eta_{struct}/1000$ (as in Figure 6) and $\beta_{jk} = (\hat{N}_j + \hat{N}_k)\omega\eta_{struct}/10$, respectively.

The non-reverberant nature of some of the subsystems is immediately apparent in the cases without coupling. For the higher frequency shown here, in Figure 7(b), the type L modes particularly are showing a very rapid spatial decay. This can be attributed mainly to their high damping (predominantly by radiation). It is no wonder, with such extreme non-reverberant behaviour, that SEA does not predict the energy distribution very accurately.

Notice in Figure 7(b) that because the type L modes show rapid spatial decay and are also coupled to the type IS modes, the resulting pattern has a local maximum near the bulkhead. What is happening is that energy initially fed into the type L modes decays rapidly, so that little of it reaches the bulkhead. However, energy reaches the bulkhead quite efficiently via the type IS modes, and some of it is then scattered into type L modes, travelling outwards from the bulkhead in both directions. These again decay rapidly, producing the local maximum.

As one would have expected, in the presence of coupling the very low levels, especially those associated with type L modes, are raised. In compensation, the rate of decay of the type IS modes becomes progressively faster, as more energy leaks out of these modes into other, more highly damped, mode types. By the case shown in Figure 7(d), all four mode types get rather rapidly locked together, and decay along parallel tracks. The particular proportions of energy in the four types when they are thus locked together are those of the eigenvector having the lowest decay rate. This is always the only eigenvector all of whose terms are positive, so that it is the only one which has physical significance in isolation. The proportions given by this eigenvector play somewhat the same role in this coupled system as does the condition of “equipartition of energy” in normal SEA: it is the state the system tends towards given sufficient length for the pattern to develop. Note that in Figures 7(c, d) two of the curves approach

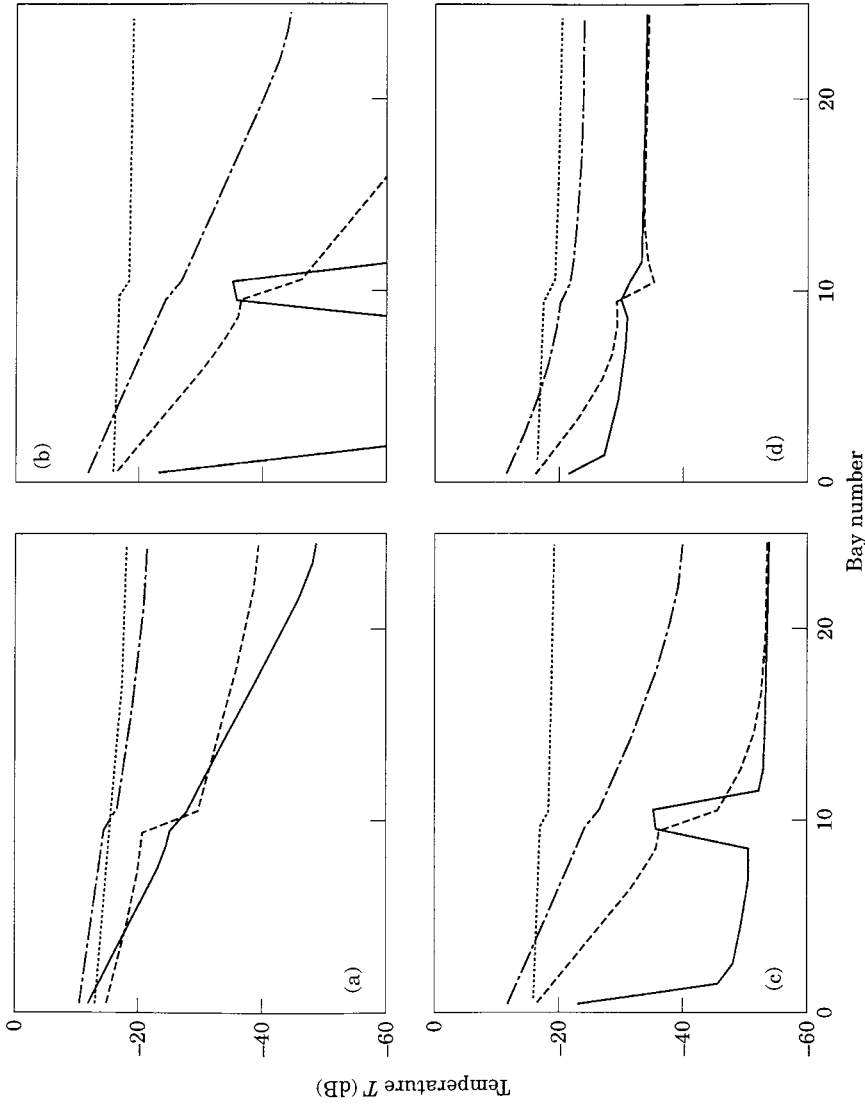


Figure 7. Spatial distribution of SEA "temperature" T_j along the two-chunk model (a) without leakage coupling, in the frequency band centred on 2250 Hz; (b) without leakage coupling, in the frequency band centred on 6250 Hz; (c) with leakage coupling $\beta_{jk} = (\hat{N}_j + \hat{N}_k)\omega\eta_{struct}/1000$, in the frequency band centred on 6250 Hz; (d) with leakage coupling $\beta_{jk} = (\hat{N}_j + \hat{N}_k)\omega\eta_{struct}/10$, in the frequency band centred on 6250 Hz. —, type L modes; - - - - -, type C modes; - · - · - ·, type R modes; · · · · ·, type IS modes.

very similar levels at higher frequencies. This is of no deep significance, simply a coincidence of the parameter values in this particular frequency band.

5. CONCLUSIONS

A statistical approach for modelling the transmission of vibration along a realistic submarine pressure hull has been developed. Fluid-loading effects are included in the modelling and are significant. Standard Statistical Energy Analysis is not adequate to deal with the rather special geometry of the submarine pressure hull, but the proposed new model captures details of behaviour which are in accordance with experimental findings. In particular, "leakage" of energy between angular orders as a result of irregularities in the hull structure can "short-circuit" a reflector such as a bulkhead or a change of frame spacing. Failure to account for this leakage in a predictive model can lead to very serious over-prediction of the effectiveness of certain vibration control measures.

The model is based on a novel subsystem breakdown, in which transmission modes on sections of the ribbed cylinder are grouped into four classes—three classes of predominantly flexural motion (having different transmission and damping characteristics) and one class of predominantly in-surface motion. In the absence of experimental data for the rates of energy leakage between these different subsystems, numerical examples have been presented which are purely illustrative of the possible behaviour. Even so, it has been clearly shown that only very small levels of leakage are required to produce significant effects on the overall pattern of vibration of a pressure hull.

ACKNOWLEDGMENTS

The authors are grateful to Dr I Roebuck of DERA for providing invaluable support, and to a referee for pointing out an error in the original version. A shorter version of this paper was presented at an IUTAM Symposium "Statistical Energy Analysis", with Proceedings published by Kluwer Academic Publishers, whose permission to use material in the present paper is gratefully acknowledged.

REFERENCES

1. M. STRASBOURG and D. FEIT 1996 *Journal of the Acoustical Society of America* **99**, 335–344. Vibration damping of a large structure induced by attached small resonant structures.
2. C. SOIZE 1993 *Journal of the Acoustical Society of America* **94**, 849–865. A model and numerical method in the medium frequency range for vibroacoustic predictions using the theory of structural fuzzy.
3. C. H. HODGES, J. POWER and J. WOODHOUSE 1985 *Journal of Sound and Vibration* **101**, 219–235. The low frequency vibration of a ribbed cylinder, part 1: theory.

4. C. H. HODGES, J. POWER and J. WOODHOUSE 1985 *Journal of Sound and Vibration* **101**, 237–256. The low frequency vibration of a ribbed cylinder, part 2: observations and interpretation.
5. D. G. CRIGHTON 1988 *Proceedings of the Institute of Acoustics* **10**(2), 1–35. The interaction between sound and vibration.
6. D. J. ALLWRIGHT, M. BLAKEMORE, P. R. BRAZIER-SMITH and J. WOODHOUSE 1994 *Philosophical Transactions of the Royal Society of London* **A346**, 511–324. Vibration transmission through symmetric resonant couplings.
7. L. CREMER, M. HECKL and E. E. UNGAR 1987 *Structure-Borne Sound*. Berlin: Springer-Verlag. See section V.6.d.
8. C. H. HODGES and J. WOODHOUSE 1986 *Reports on Progress in Physics* **49**, 107–170. Theories of noise and vibration in complex structures.
9. R. H. LYON and R. G. DE JONG 1995 *Theory and Application of Statistical Energy Analysis*. Boston: Butterworth-Heinemann.
10. K. H. HERON 1994 *Philosophical Transactions of the Royal Society of London* **A346**, 501–510. Advanced statistical energy analysis.